# Direct determination of the transition to localization of light in three dimensions

T. Sperling, [1] W. Bührer,[1] C.M. Aegerter, [2*] and G. Maret [1]

[1]Fachbereich Physik, University of Konstanz,
Universitätsstrasse 10, 78457 Konstanz, Germany

[2]Physik-Institut, University of Zürich,
Winterthurerstrasse 190, 8057 Zürich, Switzerland

In the diffusive transport of waves in three dimensional media there should be a phase transition with increasing disorder to a state where no transport occurs. This transition was first discussed by Anderson in 1958 (1) in the context of the metal insulator transition, but as was realized later it is generic for all waves (2; 3). However, the quest for the experimental demonstration of "Anderson" or "strong" localization of waves in 3D has been a challenging task. For electrons (4) and cold atoms (5), the challenge lies in the possibility of bound states in a disordered potential well. Therefore, electromagnetic and acoustic waves have been the prime candidates for the observation of Anderson localization (6–16). The main challenge using light lies in the distinction between effects of absorption and localization (10; 11). Here we present measurements of the time-dependence of the transverse width of the intensity distribution of the transmitted waves, which provides a direct measure of the localization length and is independent of absorption. From this we find direct evidence for a localization transition in three dimensions and determine the corresponding localization lengths.

In the diffusive regime ($kl^* \gg 1$) the mean square width $\sigma^2$ of the transmitted pulse, i.e. the spread of the photon cloud, is described by a linear increase in time $\sigma^2 = 4Dt$ (17). Here, $D$ is the diffusion coefficient for light, $k$ the wave-vector and $l^*$ the transport mean free path. When considering interference effects of the diffusive light, Anderson et. al (18) predicted a transition to localization in three dimensional systems at high enough turbidity $(kl^*)^{-1}$. The criterion for where this transition should occur is known as the Ioffe-Regel criterion, namely $kl^* \lesssim 1$ (19). At such high turbidities light will be localized to regions of a certain length scale, namely the localization length $\xi$, which diverges at the transition to localization. This implies that $\sigma^2$ initially increases linearly with time, but saturates at a later time $t_{\mathrm{loc}}$ (localization time) towards a constant value given by $\sigma^2 = \xi^2$, where $\xi$ is the localization length.

In this work we present measurements of light transport in 3D open, highly scattering TiO$_2$ powders. Given the high turbidity of the samples studied and the large slab thickness ($L$ varying from 0.6 mm to 1.5 mm) the transmitted light undergoes typically a few million scattering events in any of the three spatial directions before leaving the sample. Thus our samples present a true bulk 3D medium for light transport.

The great advantage of determining the time dependence of the width of the transmission profile lies in the fact that since the width is obtained at a specified time, absorption effects are present on all paths equally. This means that the width of the profile at a given time is *independent of absorption*. This can be seen from the general definition of the width in terms of the spatial dependence of the photon density $T(\rho, t)$, where $\rho$ is a vector in the 2D transmission plane with the origin at the center of the beam: $\sigma^2(t) = \int \rho^2 T(\boldsymbol{\rho}, t) \mathrm{d}^2\boldsymbol{\rho} / \int T(\boldsymbol{\rho}, t)\mathrm{d}^2\boldsymbol{\rho}$. In this definition, an exponential decrease due to absorption enters $T(\rho, t)$ both in the nominator and in the denominator and thus cancels out. In the diffusive regime, the profile will be given by a Gaussian: $T(\rho) \propto \exp(-\frac{\rho^2}{8Dt})$, i.e. with a width $\sigma^2 = 4Dt$. Hence we fit a 2D Gaussian to the intensity profile at a given time (see Fig. 1, which shows the gated intensity profile at three different time points demonstrating the increase in width with time). This fit yields the width of the Gaussian in both the x- and y-direction. In localizing samples, the intensity distribution is expected to be exponential, with a characteristic length scale $\xi$. This can be seen in our samples, however at small distances $\rho$ the profile can be well approximated by a Gaussian (see supplementary material). Hence, we fit a Gaussian to all our samples, which gives qualitatively similar fits as an exponential function in the localized case (see supplementary material).

The fitted widths are then plotted as a function of time to yield the results shown in Fig. 2 (a-c). In the case of a diffusive sample, Aldrich anatase, with $kl^*_{AA} = 6.4$, the square of the width increases linearly over the whole timespan (see Fig. 2 a) as expected. The small deviation from linearity around the diffusion time $\tau_{max}$ is a result of the gating of the high rate intensifier (HRI) (see supplementary material). The slope of the increase is in good accord with the diffusion coefficient determined from time dependent transmission experiments [13], see table 1 in the supplementary material. Note also that the time dependent width can exceed the thickness of the sample, which is a consequence of the fact that we are studying the transmission profile at specific times.

The width $\sigma^2$ of the transmitted pulse gives a direct measure of the localization length $\xi$ in the localizing regime. This is because the 2D transmission profile of the photon cloud is confined to within a localization length. When considering an effective diffusion coefficient corresponding to the slope of the temporal increase in width, one thus obtains an effective decrease of the diffusion coefficient with time as $D(t) \propto 1/t$ after a time scale corresponding to the localization length [20]. In this picture, for large $L$, one expects a time dependence

3

of $\sigma^2$, which is linear up to the localization length and then remains constant as time goes on. Numerical calculations of self-consistent theory (21; 22) give a different increase at short times as $\sigma^2 \propto t^{1/2}$ and a plateau value of $\sigma^2 = 2L\xi$ for $L \gg \xi$. These predictions can be directly tested from data of samples with high turbidity, which show non-classical diffusion in time dependent transmission measurements. This is shown in Fig. 2 b) and c). Taking a closer look at the short time behavior one can see that $\sigma^2$ increases linearly in time contrary to the self-consistent theory calculation. This is similar to the behavior found in acoustic waves (16). However in contrast to the diffusive sample, a plateau of the width can be clearly seen. This is in good accord with the theoretical prediction (22) and a direct sign of Anderson localization. This plateau can also be seen directly from the transmission profiles shown in Fig. 1, where the normalized intensity profile is shown for three different time points. At late times, the width does no longer increase indicating a localization of light.

The data shown in Fig. 2 also show results for samples of different thickness. These samples of different thickness are made from the same particles but may vary slightly in terms of filling fraction. However as checked by coherent backscattering, samples made up from the same particles have very comparable turbidity (see supplementary material). If the thickness $L$ of the sample becomes comparable to the localization length, a decrease of the width of the photon distribution with time can be observed. This surprising fact can be understood in a statistical picture of localization, where a range of localization lengths exists in the sample corresponding to different sizes of closed loops of photon transport. In finite slabs, larger localized loops may be cut off by the surfaces more likely than small loops leading to a lower population of such localized states at longer times. Thus on average, the observed width will correspond to increasingly shorter localization lengths and thus a decrease of $\sigma^2$ with time may occur. This is schematically illustrated in Fig. 2 d). Note that such a peak in the width of the intensity distribution has also been seen in calculations of self-consistent theory, albeit in thicker samples (22), such that no direct comparison with our data is possible. When the thickness decreases even more, such that it is shorter than the localization length, the plateau in the width is lost altogether and $\sigma^2$ increases over the whole time window. In fact, the behavior rather corresponds to that predicted for the mobility edge (20), where a sub-linear increase of $\sigma^2 \propto t^{2/3}$ is predicted. At the transition one observes a kink in $\sigma^2$ and the ratio of the initial slope to that at the kink corresponds to the sub-diffusive exponent $a$. In fact, this thickness dependence can be used as an alternative

4

determination of the localization length.

The evaluation of the plateaus of the localizing samples for different thicknesses yields a localization length independent of $L$. In case the time dependence showed a maximum rather than a plateau, the maximum value was used. Thus we identify $\sigma_\infty^2 = \xi^2$ and obtain $\xi_{\text{R104}} = 717(6)\mu\text{m}$ for R104, $\xi_{\text{R902}} = 717(9)\mu\text{m}$ for R902 and $\xi_{\text{R700}} = 670(9)\mu\text{m}$ for R700. These are mean values for all thicknesses investigated.

As expected, sample R700 has the smallest localization length $\xi$, as has already been concluded from time of flight experiments (13), and corresponds to the lowest value of $kl_{R700}^* = 2.7$. In terms of localization, R104 and R902 are very comparable, which again is in good accord with the fact that their turbidities are very similar, $kl_{R104}^* = 3.7$ and $kl_{R902}^* = 3.4$ respectively, even though their other sample properties are rather different. As stated above, this determination of $\xi$ is in good accord with that from the thickness dependence of the occurrence of a plateau. As seen in Fig. 2, R104 with a thickness of $L = 0.71$mm behaves sub-diffusively, but the sample with $L = 0.75$mm shows a plateau, indicating a localization length of $\xi = 0.73(2)$mm. The same transitional behavior can be seen for R902 between $0.7$mm $< L < 0.8$mm as well.

So far, we have shown that for different samples showing a range of $kl^*$ close to unity a qualitative change in the transport properties occurs which is consistent with the transition to Anderson localization. In order to show that these are not sample intrinsic properties, we now study one and the same sample at different incoming wavelengths. The turbidity depends quite strongly on the wavelength $\lambda$ of light, which we tuned from $550\,\text{nm}$ to $650\,\text{nm}$. For these wavelengths, we have determined that the turbidity changes from $kl_{550\text{nm}}^* \approx 2.1$ up to $kl_{650\text{nm}}^* \approx 3.45$, thus spanning a range similar to that of the different samples above. At the highest and lowest wavelengths, the values of $kl^*$ were interpolated from the experimentally accessible values, which is a good approximation, since for the investigated region $kl^*$ are found to scale linearly with $\lambda$ (see supplementary material). The result of such a spectral measurement of a R700 sample ($L = 0.98\,\text{mm}$ and $m = 377\,\text{mg}$) is shown in Fig. 3. For the wavelengths of $640\,\text{nm}$ and $650\,\text{nm}$, corresponding to the largest values of $kl^*$, $\sigma^2$ does not saturate while it does for smaller $kl^*$, which pin points the mobility edge. This allows a direct characterization of the localization transition with a continuous change of the control parameter $kl^*$.

We have determined the same spectral information also from a R104 sample, which is

closer to the mobility edge at a wavelength of 590 nm and for a rutile sample from Aldrich, which shows classical diffusion at 590 nm. For all of these samples, we have determined the value of $kl^*$ (23). With the value of $\xi$, and the scattering strength $kl^*$ we are able to determine the approach to the mobility edge at $kl^*_{\text{crit}}$, as shown in Fig. 4. At the mobility edge, we can determine the qualitative change in behavior from the ratio of the slopes of $\sigma^2$ as a function of time in the localized or sub-linear regime and the initial diffusive regime (see supplementary material). This gives a direct estimate of the exponent $a$ with which the width increases with time, $\sigma^2 \propto t^a$ shown in Fig. 5. There is a clear transition in the behavior with $kl^*$, showing a critical value of $kl^*_{\text{crit}} = 4.5(4)$, above which $a = 1$ and below which $a = 0$. This is in good accord with the determination from time of flight measurements on similar samples yielding $kl^*_{\text{crit,ToF}} = 4.2(2)$ (14). Note that with an effective refractive index of the samples of $n_{\text{eff}} \simeq 1.75$, a critical value of $kl^*_{\text{crit}} = 4.2$ corresponds to an onset of localization at the point of $l^*/\lambda_{\text{eff}} \approx 1$, which is a reasonable expectation for the onset of localization.

The dependence of the inverse width on the turbidity, as shown in Fig. 4, also indicates the critical behavior around the transition. Below the critical turbidity, $\sigma^2$ increases at all times and the corresponding inverse localization length is zero. At the mobility edge, the localization length is limited by the sample thickness, which in the case shown here was approximately 1 mm and a more detailed determination of the intrinsic localization length is not possible. For highly turbid samples, well below the transition, the inverse localization length seems to increase linearly with decreasing $kl^*$ indicating an exponent of unity. However, there is insufficient dynamic range close to the transition for a full determination of a critical exponent.

In conclusion, we have shown direct evidence for localization of light in three dimensions and the corresponding transition at the mobility edge. This has been achieved using the time dependence of the mean square width $\sigma^2$ of the transmission profile, which is an excellent measure for the onset of localization of light. In contrast to other measures, it is completely independent of absorption and allows a *direct* determination of the localization length for samples close to the mobility edge. We find that for highly turbid samples, $\sigma^2$ shows a plateau, which changes to a sub-linear increase for critical turbidities and becomes linear for purely diffusive samples. This allows a detailed characterization of the behavior of transport close to the transition, which is not possible with other techniques. By evaluating

the plateau $\sigma_\infty^2$ of localizing samples one can directly access the localization length $\xi$. For sample thicknesses close to the localization length, we moreover observe a decrease in the width of the photon cloud, which we associate with a statistical distribution of microscopic localization lengths. These data may stimulate further theoretical work and comparison between such quantitative theories, such as self-consistent theory (22) or direct numerical simulation (24) and the data may yield valuable information about the statistical distribution of localization lengths close to the transition.

In addition, we have shown that the transition to localization can be observed in one and the same sample using spectral measurements, thus continuously varying the control parameter of turbidity through the transition. For highly turbid samples, the width of the transmission profile saturates at a value, which increases with decreasing turbidity until the localization length is comparable to the sample thickness. At this point the width increases at all times, albeit with a sub-linear increase at long times. This behavior is expected from the diffusion coefficient at the mobility edge (20). Such measurements close to the transition between Anderson localization and diffusion allow a determination of the critical turbidity $kl_{\mathrm{crit}}^* = 4.5(4)$, which is in good agreement with an indirect determination using time of flight measurements. In addition, our determination of the localization length during the approach to the localization transition allows an estimate of the critical exponent of the transition. Well away from the critical regime, we find a value close to unity, which is not incompatible with theoretical determinations (3; 18; 25). A complete description of the transition in open media taking finite size effects into account will be a great challenge for future theoretical descriptions of Anderson localization.

**Methods**

The samples are slabs made up of nano particles of sizes ranging from 170 to 540 nm in diameter with polydispersities ranging between 25 and 45 %. Powders were provided by DuPont and Sigma Aldrich. These samples are slightly compressed and have been used previously (13) to demonstrate non-classical transport behaviour in time dependent transmission. $TiO_2$ has a relatively high refractive index in the visible of $n = 2.7$ in the rutile phase and 2.5 in the anatase phase.

The extremely high turbidity of the samples implies the use of a high power laser system to be able to measure this transmitted light. We use a frequency doubled Nd:YAG laser (Verdi V18), operated at 18 W output power, to pump a titanium sapphire laser (HP Mira).

7

The HP Mira runs mode locked with a repetition rate of 75 MHz at a maximum of about 4 W. To convert the laser light from about 790 nm to orange laser light (590 nm) a frequency doubled OPO is used. The laser wavelength emitted by the OPO can be tuned from approx. 550 nm to 650 nm.

To approximate a point-like source the laser beam was focused onto the flat front surface of the sample with a waist of 100 $\mu$m. The transmitted light was imaged from the flat backside by a magnifying lens ($f$ =25 mm, mounted in reverse position) onto a high rate intensifier (HRI, LaVision PicoStar). The HRI can be gated on a time scale of about 1 ns and the gate can be shifted in time steps of 0.25 ns. The HRI is made of gallium arsenide phosphide which has a high quantum efficiency of maximum 40.6 % at about 590 nm. A fluorescent screen images the signal onto a 16 bit CCD Camera with a resolution of 512 $\times$ 512 pixel. With this system we were able to record the transmitted profile with a time resolution below a nanosecond.

To measure the turbidity of a sample we used a backscattering set-up described elsewhere (12; 23). With this setup covering the full angular range, it is possible to determine $kl^*$ from the inverse width of the backscattering cone. Since this system used different laser sources, the spectral range of the set-up is more limited in wavelength (568 nm to 619 nm and 660 nm).

## References

1 Anderson, P.W. Absence of diffusion in certain random lattices. *Phys. Rev.* **109**, 1492-1505 (1958).

2 Anderson, P.W. The question of classical localization: a theory of white paint? *Philosophical Magazine. Lett* **52**, 505-509 (1985).

3 John, S. Electromagnetic Absorption in a Disordered Medium near a Photon Mobility Edge *Phys. Rev. Lett.* **53**, 2169-2172 (1984).

4 Altshuler, B.L. et al., Mesoscopic Phenomena in Solids (North-Holland, Amsterdam, 1991).

5 Kondov, S.S., *et al.* Three-Dimensional Anderson Localization of Ultracold Matter. *Science* **334**, 66-68 (2011).

6 Kuga, Y. and Ishimaru, A. Retroreflectance from a dense distribution of spherical particles. *J. Opt. Soc. Am. A* **1**, 831-835 (1984).

7 van Albada, M.P. and Lagendijk, A. Observation of weak localization of light in a random medium. *Phys. Rev. Lett.* **55**, 2692-2695 (1985).

8 Wolf, P.E. and Maret, G. Weak localization and coherent backscattering of photons in disordered media. *Phys. Rev. Lett.* **55**, 2696-2699 (1985).

9 Drake, J.M. and Genack, A.Z. Observation of nonclassical optical diffusion. *Phys. Rev. Lett.* **63**, 259-262 (1989).

10 Wiersma, D.S., Bartolini, P., Lagendijk, A., and Righini, R. Localization of light in a disordered medium. *Nature* **390**, 671-673 (1997).

11 Scheffold, F., Lenke, R., Tweer, R., and Maret, G. Localization or classical diffusion of light? *Nature* **398**, 206-270 (1999).

12 Fiebig, S., Aegerter, C.M., Bührer, W., Störzer, M., Akkermans, E., Montambuax, G. and Maret, G. Conservation of energy in coherent backscattering at large angles. *EPL* **81**, 64004 (2008).

13 Störzer, M., Gross, P., Aegerter, C.M. and Maret, G. Observation of the critical regime in the approach to Anderson localization of light. *Phys. Rev. Lett.* **96**, 063904 (2006).

14 Aegerter, C.M., Störzer, M. and Maret, G. Experimental determination of critical exponents in Anderson localization of light. *Europhys. Lett.* **75**, 562-568 (2006).

15 Bayer, G. and Niederdränk, T. Weak localization of acoustic waves in strongly scattering media. *Phys. Rev. Lett.* **70**, 3884-3887 (1993).

16 Hu, H., Strybulevych, A., Page, J.H., Skipetrov, S.E. and van Tiggelen, B.A. Localization of ultrasound in a three-dimensional elastic network. *Nature Phys.* **4**, 945-948 (2008).

17 Lenke, R. and Maret, G. Multiple Scattering of Light: Coherent Backscattering and Transmission *Gordon and Breach Science Publishers* (2000).

18 Abrahams E., Anderson P.W., Licciardello D.C., and Ramakrishnan T.V. Scaling theory of localization: absence of quantum diffusion in two dimensions. *Phys. Rev. Lett.* **42**, 673-676 (1979).

19 Ioffe, A.F. and Regel, A.R. Non-crystalline, amorphous and liquid electronic semiconductors. *Prog. Semicond.* **4**, 237-291 (1960).

20 Berkovits, R. and Kaveh, M. Propagation of waves through a slab near the Anderson transition: a local scaling approach. *J. Phys. C: Cond. Mat.* **2**, 307-321 (1990).

21 Skipetrov, S.E. and van Tiggelen, B.A. Dynamics of Anderson localization in open 3D media. *Phys. Rev. Lett.* **96**, 043902 (2006).

22 Cherroret, N., Skipetrov, S.E. and van Tiggelen, B.A. Transverse confinement of waves in random media. *Phys. Rev. E* **82**, 056603 (2010).

23 Gross, P., Störzer, M., Fiebig, S., Clausen, M., Maret, G. and Aegerter, C.M. A precise method to determine the angular distribution of backscattered light to high angles. *Rev. Sci. Instrum.* **78**, 033105 (2007).

24 Gentilini, S., Fratalocchi, A., and Conti, C. Signatures of Anderson localization excited by an optical frequency comb. *Phys. Rev. B.* **81**, 014209 (2010).

25 MacKinnon, A. and Kramer, B. One-parameter scaling of localization length and conductance in disordered systems. *Phys. Rev. Lett.* **47**, 1546-1549 (1981).

Author contributions: TS,WB,CMA and GM conceived and designed experiments, TS and WB carried out experiments, TS,WB,CMA and GM analysed and interpreted data, TS,WB,CMA and GM wrote the manuscript.

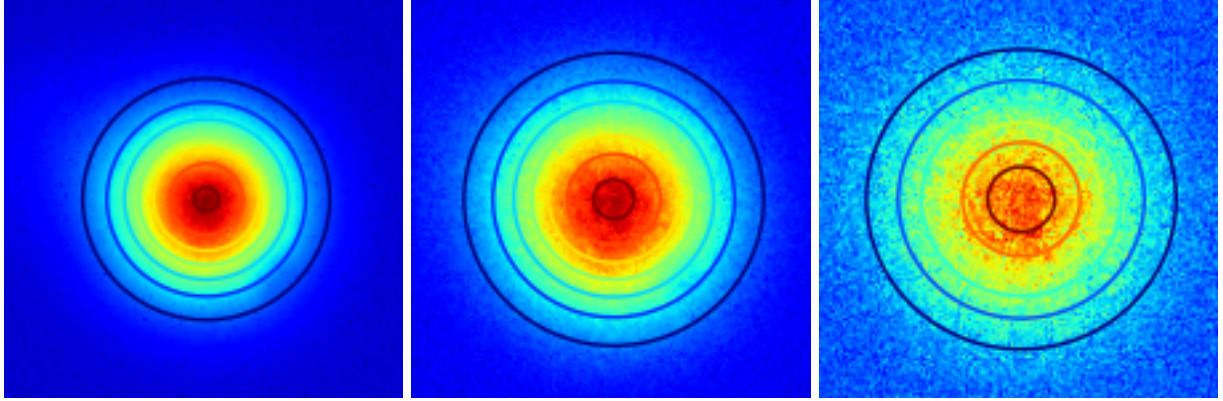Correspondence to CMA: aegerter@physik.uzh.ch

FIG. 1: This figure shows a section of the raw data (with the fit displayed via contours) of a R104 sample that features a plateau. From left to right the timestamps are 4 ns, 6 ns and 8 ns after the initial laser-pulse. From 4 ns to 6 ns one can see a broadening in the profile width, whereas from 6 ns to 8 ns no further increase can be seen. This constant profile width is the signature of Anderson localization.
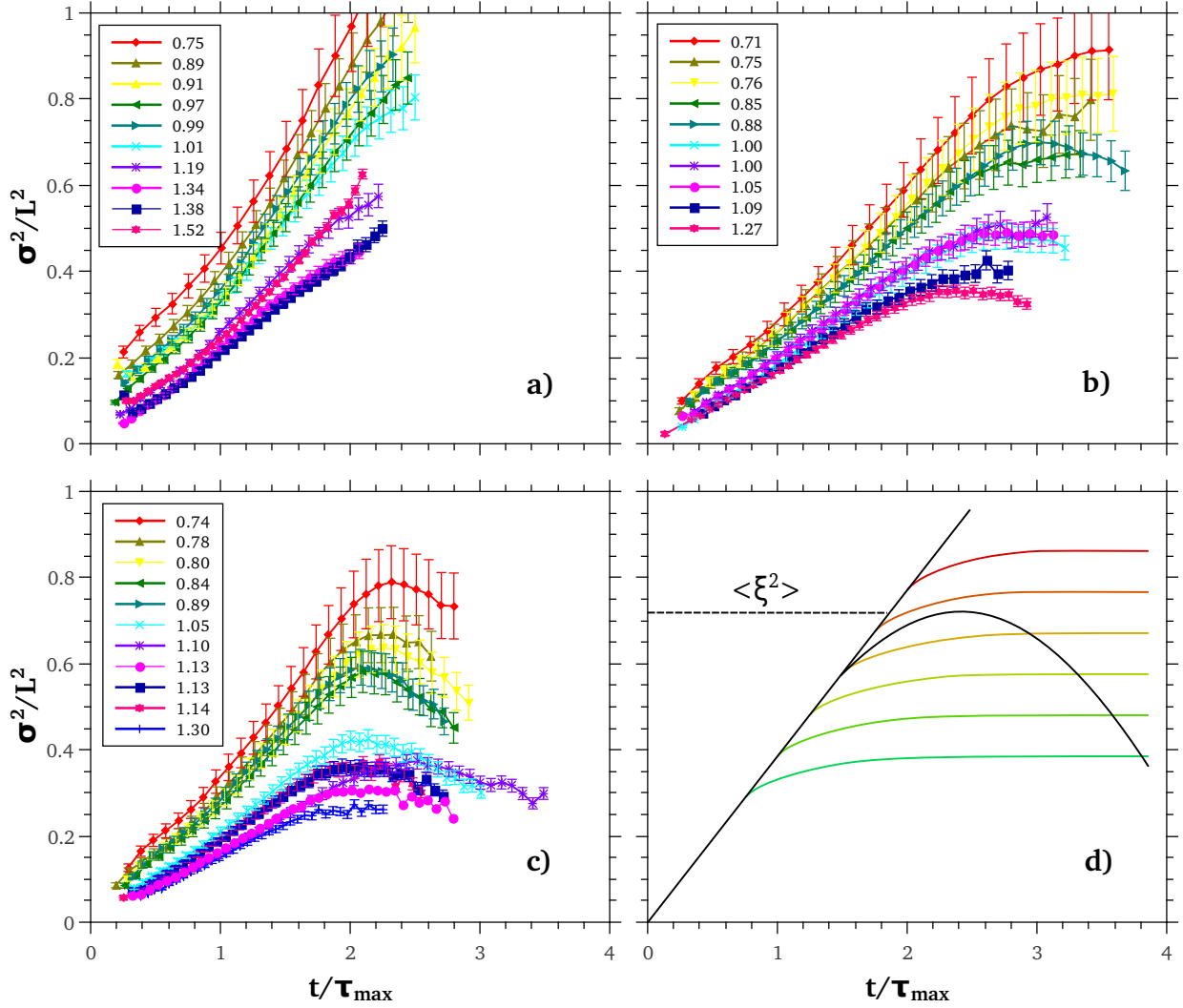
FIG. 2: The time dependence of the mean square width scaled with the sample size $\frac{\sigma^2}{L^2}$ is shown for different samples. The legends show the slab thickness $L$ in mm. The time axis is scaled with the diffusion time $\tau_{\mathrm{max}}$ (see supplementary material). In a) Aldrich anatase is shown, which behaves diffusively. Samples showing localizing effects are b) R104 and c) R700. d) Schematic illustration of the expectation for the time dependence of the width in the presence of statistically distributed localization lengths as discussed in the text. The decreasing population at late times of the modes for larger localization lengths (different colored lines belong to microscopic localization lengths increasing from small (green) to large (red)) leads to an overall decrease of the width, in particular for sample thicknesses close to the average localization length, because big loops are leaking out of the sample more than small loops.
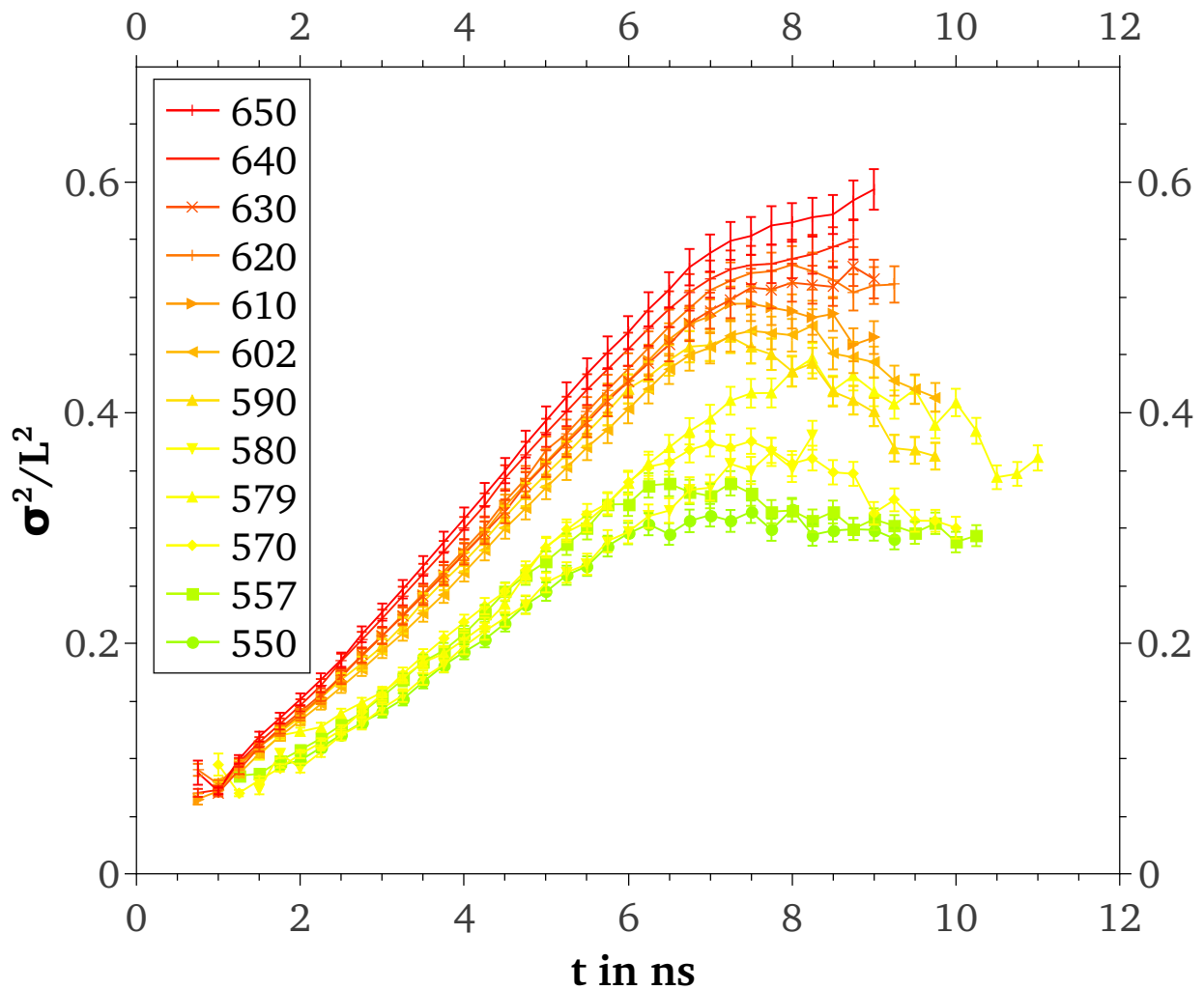
12

FIG. 3: The spectral measurement of $\sigma^2$ from a R700 sample ranging from $550\,\text{nm} - 650\,\text{nm}$, corresponding to $kl*$ values between 2.1 and 3.6, is shown. With decreasing wavelength $\lambda$ the turbidity $kl^*$ increases, as well as localizing effects are getting stronger. This can be seen via the lower mean square width $\sigma^2_\infty$ of the plateaus. For the wavelengths above $640\,\text{nm}$ one may observe a transition from localization to a sub-diffusive behavior. The legend shows the wavelength of light in nm.
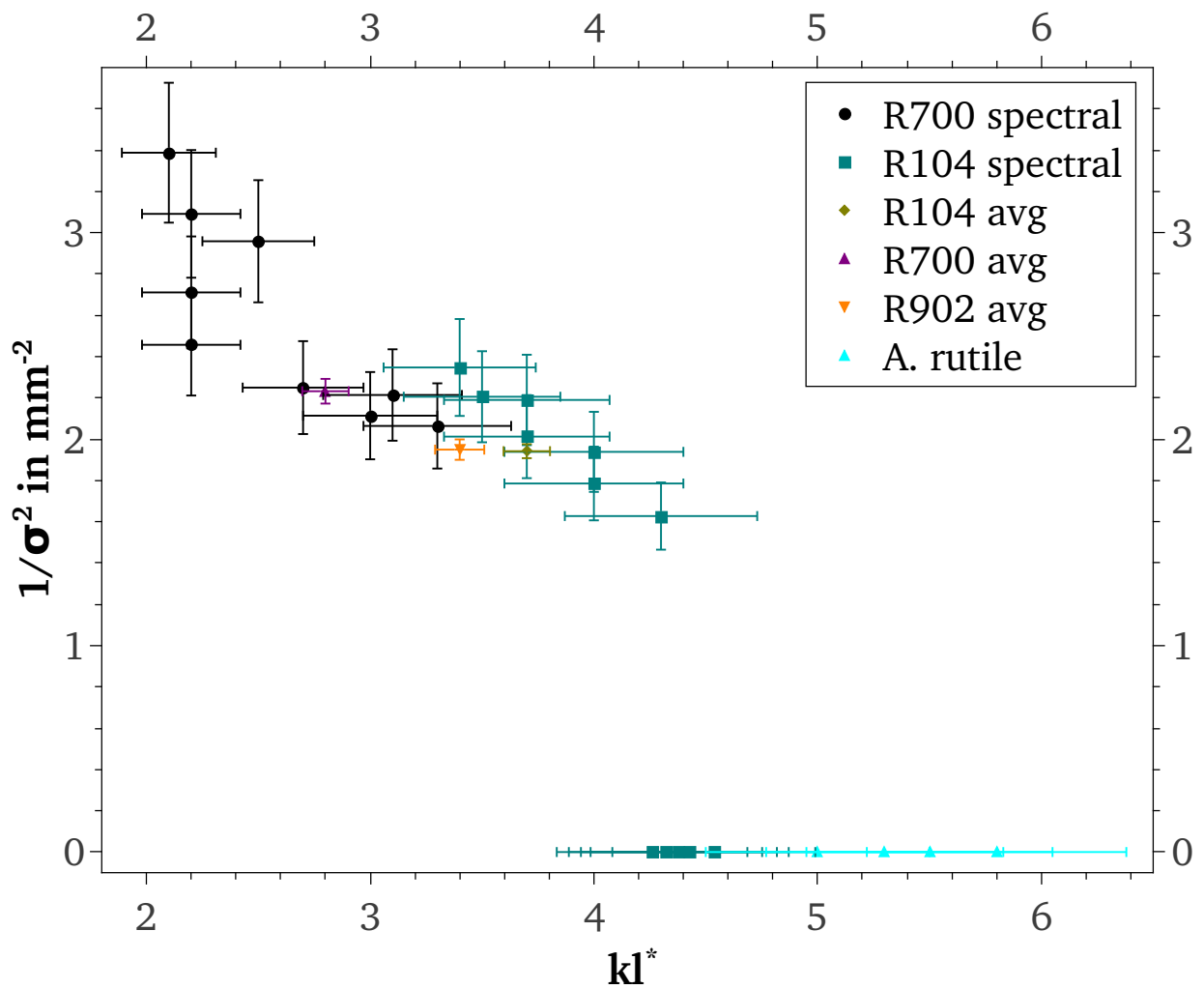
FIG. 4: The inverse of the mean square width $\sigma_\infty^2$ of the plateau against $kl^*$ for different samples. As can be seen, the width (corresponding to the localization length) diverges at a value of $kl^* \simeq 4.5$, indicating the transition from a localized to a non-localized state. The increase of the localization length approaching the critical turbidity can also be used to estimate the critical exponent.
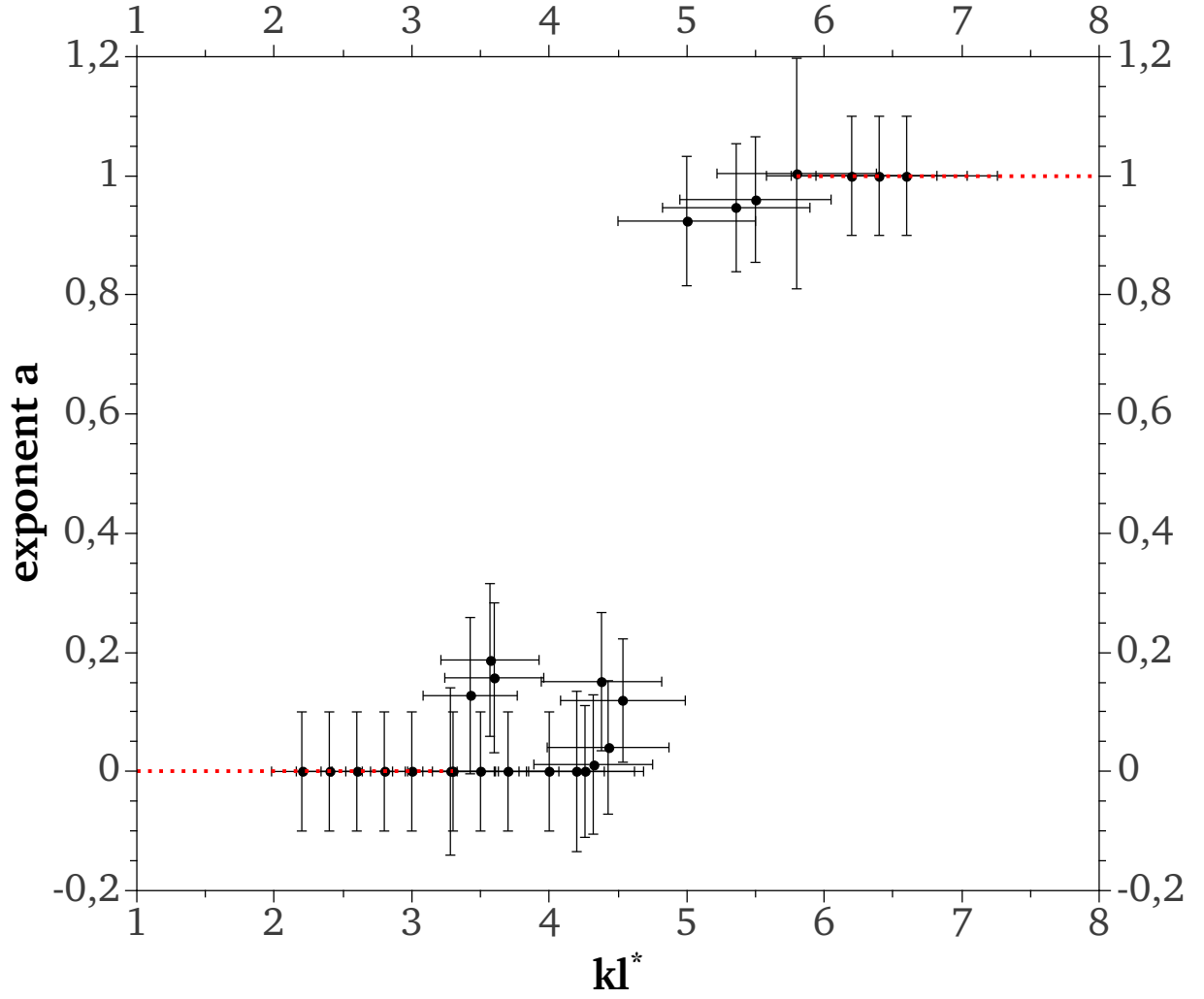
FIG. 5: The value of the exponent $a$ describing the temporal increase of the mean square width (see text). In the diffusive regime, the exponent should be unity, whereas in the fully localized regime a value of zero is expected. At the mobility edge the sub-diffusive increase corresponds to intermediate values. This allows a determination of the critical turbidity.